Graphical Abstract

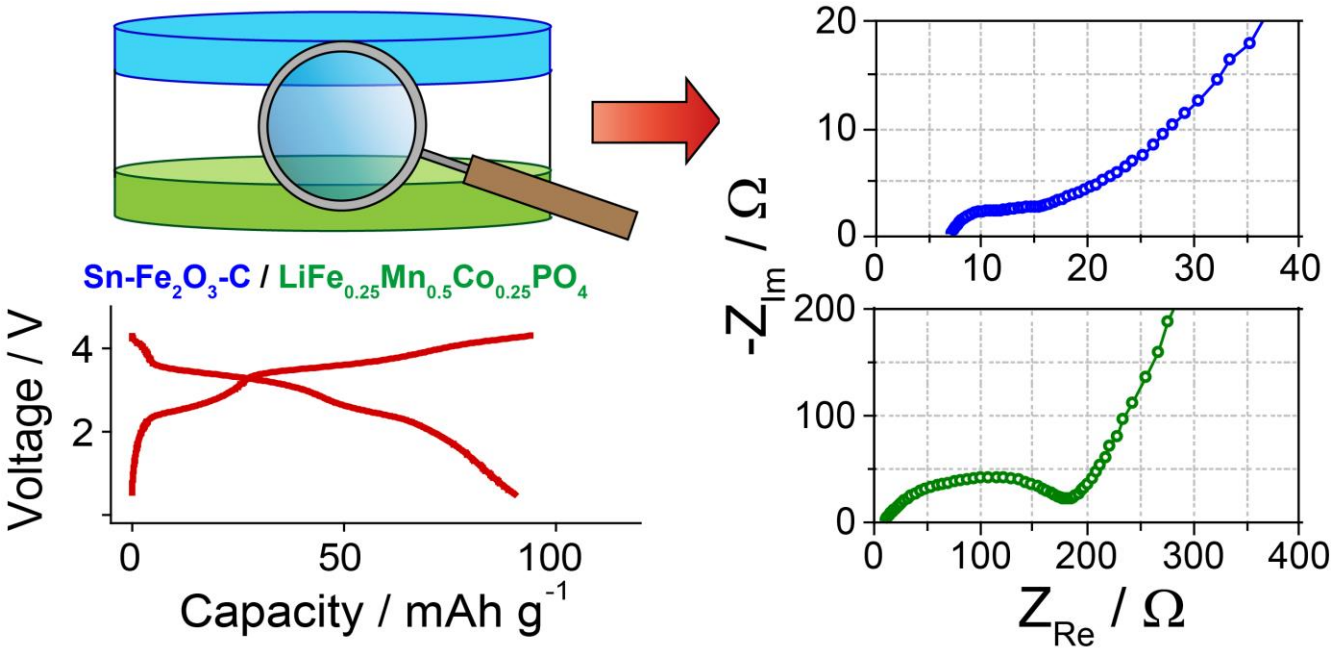

Highlights

- New Li-ion batteries are reported
- $LiFe_{0.25}Mn_{0.5}Co_{0.25}PO_4$ olivine is used as the cathode
- Either Sn-C or Sn-Fe_2O_3-C composites are used as anodes
- The electrode/electrolyte interfaces are monitored by EIS
- The systems are considered suitable for energy storage

New lithium ion batteries exploiting conversion/alloying anode and $LiFe_{0.25}Mn_{0.5}Co_{0.25}PO_4$ olivine cathode

Daniele Di Lecce[a], Roberta Verrelli[a] and Jusef Hassoun[b*]

[a] Sapienza University of Rome, Chemistry Department, Piazzale Aldo Moro, 5, 00185, Rome, Italy

[b] Department of Chemical and Pharmaceutical Sciences, Chemistry, University of Ferrara, Via Fossato di Mortara, 17, 44121, Ferrara, Italy

[*] Corresponding author: jusef.hassoun@unife.it

Abstract

New Li-ion cells are formed by combining a $LiFe_{0.25}Mn_{0.5}Co_{0.25}PO_4$ olivine cathode either with Sn-Fe_2O_3-C or with Sn-C composite anodes. These active materials exhibit electrochemical properties particularly attractive in view of practical use, including the higher working voltage of the $LiFe_{0.25}Mn_{0.5}Co_{0.25}PO_4$ cathode with respect to conventional $LiFePO_4$, as well as the remarkable capacity and rate capability of Sn-Fe_2O_3-C and Sn-C anodes. The stable electrode/electrolyte interfaces, demonstrated by electrochemical impedance spectroscopy, along with proper mass balancing and anode pre-lithiation, allow stable galvanostatic cycling of the full cells. The two batteries, namely Sn-Fe_2O_3-C/$LiFe_{0.25}Mn_{0.5}Co_{0.25}PO_4$ and Sn-C/$LiFe_{0.25}Mn_{0.5}Co_{0.25}PO_4$, reversibly operate revealing promising electrochemical features in terms of delivered capacity, working voltage and stability, thus suggesting these electrodes combinations as suitable alternatives for an efficient energy storage.

Keywords

Olivine cathode; conversion; alloy anode; impedance spectroscopy; Li-ion battery

Introduction

Urgent need for improving conventional Li-ion battery science and technology, triggered by the growing demand for energy storage, has promoted several studies on new electrodes exhibiting enhanced features with respect to state of the art battery materials [1]. Accordingly, the main approach for upgrading currently available electrodes is represented by the development of new chemistries and compositions, leading to high values of the stored capacity [2] and working voltage [3]. Anodes reacting by lithium alloying and conversion mechanisms have been proposed as viable candidates characterized by remarkable specific capacity [4]. Among the various alloying materials (*e.g.* Si, Ge, Sb, P, etc.) Sn represents a good compromise in terms of delivered capacity, material cost, toxicity, volume strain upon cycling and safety [5–7]. Indeed, while the theoretical gravimetric capacity of Sn is remarkably lower than the Si one (about 994 and 4200 mAh g^{-1} for Sn and Si, respectively), their theoretical volumetric capacities are not significantly different, being of 7233 mAh cm^{-3} and 8363 mAh cm^{-3} for Sn and Si, respectively. It is also worth mentioning that the very high specific gravimetric capacity of Si anodes, largely exceeding that of the existing cathode materials, may be disadvantageous in terms of cell balancing (i.e. anode loading, N/P ratio, etc.). In this respect, Sn anodes may represent a more viable choice than Si in full lithium-ion battery configurations. Furthermore, the volume change experienced by Sn upon reaction with Li^+ is estimated to be of about 260 %, while Si is affected by a volume expansion of about 320%. Compared to Sb, Sn exhibits higher theoretical specific capacity (about 4200 mAh g^{-1} for Sn versus 660 mAh g^{-1} for Sb) and comparable volume change during charge/discharge, i.e. about 260% and 200% for Sn and Sb, respectively. Moreover, Sn has a working voltage of about 0.3-0.4 V vs Li^+/Li, which is lower than the one ascribed to Sb (above 0.7 V vs Li^+/Li [8]), thus suggesting Sn-based anodes as the preferred choice in full cells configuration in terms of battery energy density. As for the cathode side, large attention has been devoted towards materials with working voltages much higher than conventional $LiCoO_2$ and $LiFePO_4$ [9]. However, most of these studies have focused on the electrochemical characterization of the

materials in half-cell configuration employing lithium metal anode, while only limited number of papers have demonstrated application in full Li-ion cells [5]. Indeed, the investigation of prototypes using negative and positive Li-ion electrodes may actually proof the suitability of the materials, by addressing concerns related to irreversible capacity, unstable solid electrolyte interface (SEI), and side reactions leading to cell balance loss and consequent failure [5]. Therefore, further studies aimed at determining the SEI layer stability and electrode reversibility are required in order to setup careful negative to positive (N/P) mass ratio, thus allowing proper operation and suitable cycle life of the full cell.

In this respect, we recently proposed new electrode materials for application in Li-ion battery based on lithium alloying and conversion at the anode [10–13] and lithium insertion in $LiFe_{1-\alpha}Me_{\alpha}PO_4$ olivine at the cathode [14,15]. In particular, Sn-C [10] and Sn-Fe_2O_3-C [13] anodes have shown great reliability and outstanding electrochemical performances while the $LiFe_{0.25}Mn_{0.5}Co_{0.25}PO_4$ composition has revealed higher potential vs. Li^+/Li than common $LiFePO_4$ and, contemporary, relevant reversibility and cycling ability. Following this trend, we study herein the characteristics of the materials in Sn-C/$LiFe_{0.25}Mn_{0.5}Co_{0.25}PO_4$ and Sn-Fe_2O_3-C/$LiFe_{0.25}Mn_{0.5}Co_{0.25}PO_4$ full cells. The ratio of this study principally lies in the use of new electrode combinations characterized contemporary by good electrochemical performances, as well as by expected low cost and environmental compatibility of the employed materials. The Li-ion batteries are investigated by galvanostatic cycling and compared focusing particular attention to the electrochemical characteristics of the electrode/electrolyte interface inferred from electrochemical impedance spectroscopy (EIS) and to the electrodes tuning in terms of N/P ratio.

Experimental

$LiFe_{0.25}Mn_{0.5}Co_{0.25}PO_4$, Sn-C, and Sn-$Fe_2O_3$-C samples were synthesized by following the procedures previously reported [10,13,14]. The $LiFe_{0.25}Mn_{0.5}Co_{0.25}PO_4$ material consists of sub-micrometric aggregates of elongated, platelet-like grains. Sn-C is composed by sphere-like Sn particles with an average size ranging between 10 and 50 nm, dispersed in an amorphous Carbon matrix, with an overall sub-micrometric sample morphology. The Sn-Fe_2O_3-C composite is formed by micrometric agglomerates containing nanometric Sn (≤ 10 nm) and low crystallinity Fe_2O_3 particles dispersed within carbon. The high purity degree of all the materials has been confirmed through XRD and EDS measurements [10,13,14]. The electrode films were prepared by mixing active material, polymer binder (PVdF-HFP Kynar Flex 2801 for the cathode and PVdF 6020 Solef Solvay for the anodes), and Super P Carbon (Timcal) in the weight ratio 80:10:10 %. Tetrahydrofuran (Sigma-Aldrich) and N-methyl pyrrolidone (Sigma-Aldrich) were used as solvents for cathode and anodes, respectively. The mixtures were deposited on aluminum (cathode) and copper (anodes) foils by doctor blade, casted, and dried under vacuum to obtain films of about 4 mg cm^{-2} for $LiFe_{0.25}Mn_{0.5}Co_{0.25}PO_4$, 2.5 mg cm^{-2} for Sn-C, and 2 mg cm^{-2} for Fe_2O_3-Sn-C. The electrodes were cut in the form of 10 mm diameter disks. T-type cells were assembled in Ar-filled glovebox by stacking anode, Whatman separator soaked in 1 M $LiPF_6$ ethylene carbonate-dimethyl carbonate electrolyte (LP30, BASF), and cathode.

Electrochemical impedance spectroscopy (EIS) was carried out on three-electrode cell configuration using a lithium probe as the reference electrode and a lithium disk as the counter electrode. EIS was performed at open circuit voltage (OCV), after 1, 10, and 40 cycles of galvanostatic cycling through a VersaSTAT MC Princeton Applied Research (PAR) analyzer, by applying a 10 mV amplitude signal in the 500 kHz − 20 mHz frequency range. The EIS spectra were analyzed by nonlinear least-square (NLLS) fit [16] by using the Boukamp program. Galvanostatic cycling were performed on two-electrodes cells through a MACCOR series 4000 battery test system, with additional constant voltage step for Sn-C/$LiFe_{0.25}Mn_{0.5}Co_{0.25}PO_4$. Prior to full-cells assembling, the anodes were

partially pre-lithiated by galvanostatic cycling in order to avoid first-cycle irreversible capacity and ensure steady-state behavior. All the measurements were carried out at room temperature.

Results and discussion

The electrochemical features of the electrodes are studied by galvanostatic cycling and EIS measurements. The electrochemical system used for the tests consists of a three electrode T-type cell using a lithium foil reference probe, the active material as the working electrode and a lithium foil as the counter electrode. This configuration contemporary allows suitable cycling behavior and proper evaluation of the electrode/electrolyte interface by EIS (see the experimental section). Fig. 1 shows respectively the voltage profiles and cycling trends of $LiFe_{0.25}Mn_{0.5}Co_{0.25}PO_4$ at C/5 rate (1C = 170 mA g^{-1}; Fig. 1a, b), Sn-C at C/4 rate (1C = 400 mA g^{-1}; Fig. 1c, d), and Sn-Fe_2O_3-C at 1C rate (1C = 810 mA g^{-1}; Fig. 1e, f), i.e., at current rates that ensure optimal cycling conditions. $LiFe_{0.25}Mn_{0.5}Co_{0.25}PO_4$ reveals in lithium cell an average working voltage of 3.9 V and delivers a capacity ranging from 80 to 90 mAh g^{-1}, i.e., a lower value with respect to that observed in two electrodes cell typically employed for the galvanostatic tests (120 mAh g^{-1}) [7]. The lower value of delivered capacity may be reasonably due to the differences between the three-electrodes and two-electrodes cell set-up (including, for example, different amounts of electrolyte solution and employed separators). Furthermore, the lithium probe used as reference electrode for the EIS tests in three-electrode configuration may alter the cell geometry (increase of the thickness, change of the electric field), thus leading to a higher cell polarization in galvanostatic cycling. This lithium probe is not employed for the cycling tests of Fig. 1 which is performed in a two-electrode configuration by using only the active material as the working electrode and a lithium disk acting both as the reference and the counter electrode in a T-type cell (see the experimental section for further details). Instead, Sn-Fe_2O_3-C and Sn-C show a relevant performance with average working voltage of about 0.5 V and 1 V, respectively, and reversible

capacity as high as 400 mAh g^{-1} and 1000 mAh g^{-1}, i.e., values only slightly affected by the cell configuration [10,11].

Figure 1

The EIS responses of the above discussed lithium cells, taken at the OCV and upon cycling, are reported in Fig. 2. The Nyquist impedance plots have been analyzed by NNLS fit [16] using the equivalent circuit reported in Table 1a, formed by high frequency resistive element describing the ohmic electrolyte resistance, in series with high-middle sub-circuit element accounting for the resistance and charge transfer pseudo-capacitance at the electrode-electrolyte interface layer, in series with a low frequency Warburg element (Q_g) representative of the solid state Li^+ diffusion within the active material [17,18]. The sub-circuit element associated to the resistance and pseudo-capacitance of the interface layer is composed by a series of three elements, each consisting in a resistive (R_i) and pseudo-capacitance (Q_i) member connected in parallel. The attribution of each of these (R_iQ_i) elements to a specific interface phenomenon may not be unambiguous. We suggest that the different anode components, each exhibiting its characteristic particle size, crystallinity and chemical reactivity toward the electrolyte, may account for different time constant interface phenomena, i.e. different high-middle frequency semi-circles in the Nyquist plot. Indeed, the analysis of the interface phenomena we propose for the tested composite anodes and the equivalent circuit accordingly used are in line with other literature works on similar materials [19,20]. As for the cathode EIS characterization, a simpler equivalent circuit is used to fit the obtained Nyquist plot. The interface phenomena are described by one (RQ) element. Contributions of different components to the overall electrode-electrolyte interface resistance and charge transfer pseudo-capacitance resulting in more semi-circles overlapped within the same frequency region may not be excluded.

At the OCV condition all the electrodes show a single semicircle in the Nyquist plot, most likely related to a native passivation layer (see Fig. 2a-c). The impedance response evolves by the following cycles, owing to changes of the time-constants related to the interface phenomena, generally leading to an additional medium-frequency semicircle due to electrode charge transfer. Further medium-high semicircle may be ascribed to the heterogeneous nature of the composite electrode in terms of particle size and coating thickness distribution [21–23], as indeed observed for Sn-C (Fig. 2b) and Sn-Fe_2O_3-C (Fig. 2c). Possible overlapping of the semicircles at the medium and medium-high frequency regions may be also observed, in particular for the $LiFe_{0.25}Mn_{0.5}Co_{0.25}PO_4$ cathode (Fig. 2a). The results of NNLS fit, reported in Table 1, indicate for $LiFe_{0.25}Mn_{0.5}Co_{0.25}PO_4$ an increase of the interfacial resistance from 180 Ω at the 1st cycle to 425 Ω at the 40th cycle, mostly due to the electrolyte decomposition at the higher voltages (cell charge cutoff) and formation of favorable electrode/electrolyte interface on the cathode surface, as indeed suggested by the corresponding cycling trend (Fig 1b). Several factors may affect the evolution of the interface upon cycling, including the decomposition of the electrolyte salt, possible nucleophilic attack of the electrolyte, oxygen release and metal dissolution. Indeed, $LiPF_6$ may indeed decompose in presence of water leading to the formation of LiF, PF_5 and HF, which may react at the cathode/electrolyte interface to form LiF-like species and favor the transition metal dissolution [24]. The Nyquist plot of the Sn-C electrode (Fig. 2b) clearly reveals lower resistance values, hence highlighting fast kinetics at the electrode/electrolyte interface. The plots of Fig. 2b show a contribution of passivation layer and charge transfer to the overall interface resistance, increasing from 18 Ω at the 1st cycle to 80 Ω at the 40th cycle (see Table 1b), i.e., values ensuring a stable cycling (Fig. 1c, d).

The results of the NNLS fit of the impedance data, reported in Table 1, reveal that the overall interface resistance of the ternary Sn-Fe_2O_3-C composite does not exhibit significant variation upon cycling: the total resistance value is estimated to be as low as about 20-30 Ohm even after 40 galvanostatic cycles.

Although not being exhaustive, the EIS response upon prolonged cycling of the ternary Sn-Fe_2O_3-C composite anode (reported in Fig. 2 c as Nyquist plot and in Table 1 as fitted resistance values) may suggest reasonably high stability of the electrode SEI layer during cycling. Furthermore, considering the very low overall resistance, i.e., of about 20 Ω for 40 cycles, evidenced by Fig. 2c we may expect a well conducting Sn-Fe_2O_3-C/electrolyte interface, which accounts for the remarkable reversibility of the electrode (about 1000 mAh g^{-1}, Fig. 1e, f).

Several works have investigated the SEI layer formed on the surface of Sn-based anodes. XPS and IR measurements revealed that the SEI in conventional solutions of $LiPF_6$ salt in carbonate solvents mainly consists of lithium alkyl-carbonates, RCO_2Li, ROLi, oligomers, Li_2CO_3 and LiF with composition changing by cycles [24,25]. XPS and TOF-SIMS study on Sn-Co alloying electrodes has revealed an increase of the Li_2CO_3 content in the SEI layer upon charge/discharge cycles as well as the formation of fractures within the interface layers [26]. The exploitation of composite electrode configurations, coatings or/and electrolyte additives may reasonably stabilize the SEI layer on the electrode surface during cycling [27]. Indeed, the limited changes at increasing cycles of the Sn-C and Sn-Fe_2O_3-C interface resistance values, as revealed from EIS measurements, proof the relatively high stability of the interface layers formed by these electrodes upon prolonged cycling when electrolytes based on $LiPF_6$ salt and carbonate solvents are used. This result is in line with other experimental evidences reported in literature for similar composite materials [28,29].

Figure 2

In summary, the interface characterization suggests the applicability of the electrode combination in full cells with electrochemical features reflecting the anode and cathode properties. Accordingly, the Sn-C and Sn-Fe_2O_3-C materials exchange lithium ions in electrochemical cells at different potentials vs. Li^+/Li with specific capacities of about 400 mAh g^{-1} and 1000 mAh g^{-1}, respectively, owing to the reaction mechanisms [10,13]:

$$4.4\ Li^+ + 4.4\ e^- + Sn \rightarrow Li_{4.4}Sn \quad (1)$$

$$Fe_2O_3 + x\ Li^+ + x\ e^- \rightarrow Li_xFe_2O_3 \qquad 0 \leq x \leq 1 \quad (2)$$

$$Li_xFe_2O_3 + y\ Li^+ + y\ e^- \rightarrow Li_{x+y}Fe_2O_3 \qquad 0 \leq y \leq 1 \quad (3)$$

$$Li_2Fe_2O_3 + 4\ Li^+ + 4\ e^- \rightarrow 3\ Li_2O + 2\ Fe \quad (4)$$

$$z\ Li^+ + z\ e^- + C \rightarrow Li_zC \quad (5)$$

Mandatory steps to avoid full-cell irreversibility and ensure proper operation are represented by the careful electrodes mass balancing and the optimization of a pre-lithiation procedure of the anode [10,13]. Anode pre-lithiation before full cell assembly allows the formation of a stable SEI without irreversible consumption of Li^+ at the cathode side, thus ensuring high reversibility and coulombic efficiency of the battery even from the first cycles. The effects of pre-lithiation over the anode SEI layer evolution upon cycling and the battery performances have been deeply investigated so far through several techniques, including both in-situ and ex-situ analysis [30]. Both the Sn-C and Sn-Fe_2O_3-C anodes studied in this work are characterized by large irreversibility during the first cycles, which is in part intrinsic to the alloying and conversion chemistry and, in part, is due to the electrolyte decomposition reaction at the electrode surface with consequent formation of a SEI layer. Therefore, the stabilization of these electrodes before full cell assembly by pre-lithiation process is of definite importance in order to achieve satisfactory battery performances in terms of delivered capacity, coulombic efficiency and cycle life. The pre-lithiation may be performed electrochemically by cycling the electrodes in lithium half-cells until stationary working conditions are reached, i.e., the procedure adopted in this work, or chemically by direct contact under pressing of the electrode with lithium metal just before cell assembling [13,31].

Fig. 3a and b compare the voltage profile of $LiFe_{0.25}Mn_{0.5}Co_{0.25}PO_4$ with that of partially lithiated Sn-C (a) and Sn-Fe_2O_3-C (b). Prior to full-cell assembly, half cells were pre-cycled at current

rates allowing the maximum practical capacity of the electrodes, i.e., C/10, C/4, and 1C for $LiFe_{0.25}Mn_{0.5}Co_{0.25}PO_4$, Sn-C, and Sn-$Fe_2O_3$-C, respectively. The combination of anodes and cathode profiles leads to the voltage signature of the two full-cells reported in Fig. 3c. The Sn-Fe_2O_3-C/$LiFe_{0.25}Mn_{0.5}Co_{0.25}PO_4$ cell has a lower and more sloping voltage profile with respect to the Sn-C/$LiFe_{0.25}Mn_{0.5}Co_{0.25}PO_4$ one, as expected by the higher potential vs. Li^+/Li of the Fe_2O_3 conversion reaction compared to Li-Sn alloying process [10,13]. Accordingly, different voltage cutoffs have been set for cycling the above mentioned two full-cells. Despite the lower energy content of partially lithiated Li_x(Sn-C) and Li_x(Sn-Fe_2O_3-C) in full cell (about 200 mAh g^{-1} and 450 mAh g^{-1}, respectively), the pre-cycling process allows the evolution of the anode reaction at the lower potentials (Fig. 3a, b) and leads to higher voltage in full cells operating according to the reaction mechanisms:

$$Li_x(Sn\text{-}C) + LiFe_{0.25}Mn_{0.5}Co_{0.25}PO_4 \rightleftharpoons Li_ySn + Li_zC + Fe_{0.25}Mn_{0.5}Co_{0.25}PO_4 \quad (6)$$

$$(y = x + 1 - z \leq 4.4)$$

$$Li_x(Sn\text{-}Fe_2O_3\text{-}C) + LiFe_{0.25}Mn_{0.5}Co_{0.25}PO_4 \rightleftharpoons 3Li_2O + 2Fe + Li_ySn + Li_zC + Fe_{0.25}Mn_{0.5}Co_{0.25}PO_4 \quad (7)$$

$$(y = x - 5 - z \leq 4.4)$$

The materials indicated by Li_x(Sn-C) and Li_x(Sn-Fe_2O_3-C) may contain lithiated alloying material and carbon, lithium oxide or metallic iron, depending on the extent of the preliminary activation process of the corresponding electrode.

Figure 3

Fig. 4 shows the galvanostatic behavior at C/5 rate with respect to the cathode mass (1C = 170 mA g^{-1}) of the Sn-C/$LiFe_{0.25}Mn_{0.5}Co_{0.25}PO_4$ and Sn-Fe_2O_3-C/$LiFe_{0.25}Mn_{0.5}Co_{0.25}PO_4$ full-cells in terms of voltage profiles (a, b) and cycling trends (c). Both panels a and b of Fig. 4 actually reveal the voltage profile expected by the reactions (5) and (6), respectively, however with a progressive change by cycling likely due to partial modification of the cell balance by minor irreversibility not completely

addressed by the pre-lithiation process. Fig. 4c indicates a relatively stable cycling trend for both the Sn-C/$LiFe_{0.25}Mn_{0.5}Co_{0.25}PO_4$ and Sn-Fe_2O_3-C/$LiFe_{0.25}Mn_{0.5}Co_{0.25}PO_4$ configurations, with a steady state reversible capacity ranging from 90 to 100 mAh g^{-1} with respect to the cathode mass, thus demonstrating the reliability of the two systems. Taking into account an average operating voltage of about 3.5 and 3.2 V, and a correction factor for inactive materials contributions of 1/3, we may estimate for Sn-C/$LiFe_{0.25}Mn_{0.5}Co_{0.25}PO_4$ and Sn-Fe_2O_3-C/$LiFe_{0.25}Mn_{0.5}Co_{0.25}PO_4$ cells a practical energy density content of about 120 and 100 Wh kg^{-1} for the, respectively, which is lower than the one ascribed to commercial lithium-ion batteries based on graphite anode and $LiCoO_2$ and $LiFePO_4$ cathodes. However, the good electrochemical performances, the low cost and the environmental compatibility of the electrodes well justify the study of the battery combination here proposed.

Figure 4

Conclusions

We proposed the combination of a new $LiFe_{0.25}Mn_{0.5}Co_{0.25}PO_4$ cathode material having olivine structure with advanced conversion/alloying anodes as full Li-ion cells. The materials were studied by using an electrochemical approach coupling impedance spectroscopy and galvanostatic cycling. The results revealed suitable features of the electrode/electrolyte interface for $LiFe_{0.25}Mn_{0.5}Co_{0.25}PO_4$, Sn-C, and Sn-$Fe_2O_3$-C. The Sn-C and Sn-$Fe_2O_3$-C anodes have different electrochemical characteristics, i.e., reversible capacities of about 400 and 1000 mAh g^{-1}, respectively, and voltage signatures reflecting the Li/Sn alloying and Li/Fe_2O_3 conversion reactions. The Sn-C/$LiFe_{0.25}Mn_{0.5}Co_{0.25}PO_4$ and Sn-Fe_2O_3-C/$LiFe_{0.25}Mn_{0.5}Co_{0.25}PO_4$ cells revealed voltage profiles resulting by proper cathode/anode mass balance and anode partial pre-lithiation process. Despite the lower energy density with respect to the benchmarks, the battery prototypes preliminarily studied in this work exhibit promising features that may be optimized by further efforts aimed to improve the overall cycling performances and energy density. Indeed, the $LiFe_{0.25}Mn_{0.5}Co_{0.25}PO_4$ cathode represents a more sustainable alternative to

conventional $LiCoO_2$ cathodes in terms of environmental impact and costs. It is also worth mentioning that electrochemically de-lithiated $LiCoO_2$ is affected by poor thermal stability, with decomposition starting at about 240°C (see ref. [32] for more details), which represents a major limit toward the exploitation of its full capacity in practical batteries. When compared to conventional $LiFePO_4$, an advantage of the $LiFe_{0.25}Mn_{0.5}Co_{0.25}PO_4$ cathode lies in its higher average working voltage, *i.e.* about 4.1 and 3.4 V vs Li^+/Li for $LiFe_{0.25}Mn_{0.5}Co_{0.25}PO_4$ and $LiFePO_4$, respectively. As for the anode side, the Sn-C and Sn-Fe_2O_3-C composites deliver very high values of reversible specific capacity (much higher than that of conventional graphite electrodes of about 370 mAh g^{-1}). Moreover, these anodes are prepared through simple and sustainable preparation routes and represent a viable and low cost choice for application in batteries. Another advantage of these Sn-based anodes is represented by the high safety level even at very high cycling rates, due to their working voltage preventing possible Li deposition phenomena. Furthermore, the cell configuration proposed in this work may be attractive for application requiring low temperatures (including, for example, the electric vehicles technology), i.e., under operative conditions that suppress the intercalation ability of conventional graphite anodes. Therefore, the cells here proposed may be proposed by further optimization as alternative energy storage systems of definite interest.

Acknowledgements

The work was performed within the collaboration project "Accordo di Collaborazione Quadro 2015" between University of Ferrara (Department of Chemical and Pharmaceutical Sciences) and Sapienza University of Rome (Chemistry Department).

References

[1] L. Croguennec, M.R. Palacin, Recent Achievements on Inorganic Electrode Materials for Lithium-Ion Batteries, J. Am. Chem. Soc. 137 (2015) 3140–3156. doi:10.1021/ja507828x.

[2] B. Scrosati, J. Hassoun, Y.-K. Sun, Lithium-ion batteries. A look into the future, Energy Environ. Sci. 4 (2011) 3287. doi:10.1039/c1ee01388b.

[3] M. Hu, X. Pang, Z. Zhou, Recent progress in high-voltage lithium ion batteries, J. Power Sources. 237 (2013) 229–242. doi:10.1016/j.jpowsour.2013.03.024.

[4] J. Hassoun, B. Scrosati, Review—Advances in Anode and Electrolyte Materials for the Progress of Lithium-Ion and beyond Lithium-Ion Batteries, J. Electrochem. Soc. 162 (2015) A2582–A2588. doi:10.1149/2.0191514jes.

[5] V. Aravindan, Y.-S. Lee, S. Madhavi, Research Progress on Negative Electrodes for Practical Li-Ion Batteries: Beyond Carbonaceous Anodes, Adv. Energy Mater. 5 (2015) 1402225. doi:10.1002/aenm.201402225.

[6] S. Goriparti, E. Miele, F. De Angelis, E. Di Fabrizio, R. Proietti Zaccaria, C. Capiglia, Review on recent progress of nanostructured anode materials for Li-ion batteries, J. Power Sources. 257 (2014) 421–443. doi:10.1016/j.jpowsour.2013.11.103.

[7] N. Nitta, G. Yushin, High-Capacity Anode Materials for Lithium-Ion Batteries: Choice of Elements and Structures for Active Particles, Part. Part. Syst. Charact. 31 (2014) 317–336. doi:10.1002/ppsc.201300231.

[8] T. Ramireddy, M.M. Rahman, T. Xing, Y. Chen, A.M. Glushenkov, Stable anode performance of an Sb–carbon nanocomposite in lithium-ion batteries and the effect of ball milling mode in the course of its preparation, J. Mater. Chem. A. 2 (2014) 4282. doi:10.1039/c3ta14643j.

[9] A. Kraytsberg, Y. Ein-Eli, Higher, Stronger, Better… A Review of 5 Volt Cathode Materials for Advanced Lithium-Ion Batteries, Adv. Energy Mater. 2 (2012) 922–939. doi:10.1002/aenm.201200068.

[10] J. Hassoun, G. Derrien, S. Panero, B. Scrosati, A Nanostructured Sn-C Composite Lithium Battery Electrode with Unique Stability and High Electrochemical Performance, Adv. Mater. 20 (2008) 3169–3175. doi:10.1002/adma.200702928.

[11] R. Verrelli, J. Hassoun, A. Farkas, T. Jacob, B. Scrosati, A new, high performance CuO/LiNi0.5Mn1.5O4 lithium-ion battery, J. Mater. Chem. A. 1 (2013) 15329. doi:10.1039/c3ta13960c.

[12] R. Verrelli, J. Hassoun, High-Capacity NiO-(Mesocarbon Microbeads) Conversion Anode for Lithium-Ion Battery, ChemElectroChem. 2 (2015) 988–994. doi:10.1002/celc.201500069.

[13] R. Verrelli, J. Hassoun, High capacity tin–iron oxide-carbon nanostructured anode for advanced lithium ion battery, J. Power Sources. 299 (2015) 611–616. doi:10.1016/j.jpowsour.2015.09.034.

[14] D. Di Lecce, R. Brescia, A. Scarpellini, M. Prato, J. Hassoun, A High Voltage Olivine Cathode for Application in Lithium-Ion Batteries, ChemSusChem. 9 (2016) 223–230. doi:10.1002/cssc.201501330.

[15] D. Di Lecce, J. Hassoun, Lithium Transport Properties in LiMn 1−α Fe α PO 4 Olivine Cathodes, J. Phys. Chem. C. 119 (2015) 20855–20863. doi:10.1021/acs.jpcc.5b06727.

[16] B.A. Boukamp, A Nonlinear Least Squares Fit procedure for analysis of immittance data of electrochemical systems, Solid State Ionics. 20 (1986) 31–44. doi:10.1016/0167-2738(86)90031-7.

[17] D. Aurbach, Review of selected electrode–solution interactions which determine the performance of Li and Li ion batteries, J. Power Sources. 89 (2000) 206–218. doi:10.1016/S0378-7753(00)00431-6.

[18] B.-Y. Chang, S.-M. Park, Electrochemical Impedance Spectroscopy, Annu. Rev. Anal. Chem. 3

(2010) 207–229. doi:10.1146/annurev.anchem.012809.102211.

[19] C. Liu, H. Huang, G. Cao, F. Xue, R.A. Paredes Camacho, X. Dong, Enhanced Electrochemical Stability of Sn-Carbon Nanotube Nanocapsules as Lithium-Ion Battery Anode, Electrochim. Acta. 144 (2014) 376–382. doi:10.1016/j.electacta.2014.07.068.

[20] X. Huang, S. Cui, J. Chang, P.B. Hallac, C.R. Fell, Y. Luo, et al., A Hierarchical Tin/Carbon Composite as an Anode for Lithium-Ion Batteries with a Long Cycle Life, Angew. Chemie Int. Ed. 54 (2015) 1490–1493. doi:10.1002/anie.201409530.

[21] M.D. Levi, D. Aurbach, Impedance of a Single Intercalation Particle and of Non-Homogeneous, Multilayered Porous Composite Electrodes for Li-ion Batteries, J. Phys. Chem. B. 108 (2004) 11693–11703. doi:10.1021/jp0486402.

[22] D. Aurbach, M.D. Levi, E. Levi, A review on the solid-state ionics of electrochemical intercalation processes: How to interpret properly their electrochemical response, Solid State Ionics. 179 (2008) 742–751. doi:10.1016/j.ssi.2007.12.070.

[23] S.-D. Xu, Q.-C. Zhuang, L.-L. Tian, Y.-P. Qin, L. Fang, S.-G. Sun, Impedance Spectra of Nonhomogeneous, Multilayered Porous Composite Graphite Electrodes for Li-Ion Batteries: Experimental and Theoretical Studies, J. Phys. Chem. C. 115 (2011) 9210–9219. doi:10.1021/jp107406s.

[24] M. Gauthier, T.J. Carney, A. Grimaud, L. Giordano, N. Pour, H.-H. Chang, et al., Electrode–Electrolyte Interface in Li-Ion Batteries: Current Understanding and New Insights, J. Phys. Chem. Lett. 6 (2015) 4653–4672. doi:10.1021/acs.jpclett.5b01727.

[25] D.M. Seo, C.C. Nguyen, B.T. Young, D.R. Heskett, J.C. Woicik, B.L. Lucht, Characterizing Solid Electrolyte Interphase on Sn Anode in Lithium Ion Battery, J. Electrochem. Soc. 162

(2015) A7091–A7095. doi:10.1149/2.0121513jes.

[26] J.-T. Li, J. Swiatowska, A. Seyeux, L. Huang, V. Maurice, S.-G. Sun, et al., XPS and ToF-SIMS study of Sn–Co alloy thin films as anode for lithium ion battery, J. Power Sources. 195 (2010) 8251–8257. doi:10.1016/j.jpowsour.2010.07.043.

[27] N. Liu, Z. Lu, J. Zhao, M.T. McDowell, H.-W. Lee, W. Zhao, et al., A pomegranate-inspired nanoscale design for large-volume-change lithium battery anodes, Nat. Nanotechnol. 9 (2014) 187–192. doi:10.1038/nnano.2014.6.

[28] Y. Xu, Q. Liu, Y. Zhu, Y. Liu, A. Langrock, M.R. Zachariah, et al., Uniform Nano-Sn/C Composite Anodes for Lithium Ion Batteries, Nano Lett. 13 (2013) 470–474. doi:10.1021/nl303823k.

[29] G.A. Elia, U. Ulissi, F. Mueller, J. Reiter, N. Tsiouvaras, Y.-K.K. Sun, et al., A Long-Life Lithium Ion Battery with Enhanced Electrode/Electrolyte Interface by Using an Ionic Liquid Solution, Chem. - A Eur. J. 22 (2016) 6808–6814. doi:10.1002/chem.201505192.

[30] M.W. Forney, M.J. Ganter, J.W. Staub, R.D. Ridgley, B.J. Landi, Prelithiation of Silicon–Carbon Nanotube Anodes for Lithium Ion Batteries by Stabilized Lithium Metal Powder (SLMP), Nano Lett. 13 (2013) 4158–4163. doi:10.1021/nl401776d.

[31] J. Hassoun, K.-S. Lee, Y.-K. Sun, B. Scrosati, An advanced lithium ion battery based on high performance electrode materials., J. Am. Chem. Soc. 133 (2011) 3139–3143. doi:10.1021/ja110522x.

[32] D. Di Lecce, C. Fasciani, B. Scrosati, J. Hassoun, A Gel–Polymer Sn–C/LiMn 0.5 Fe 0.5 PO 4 Battery Using a Fluorine-Free Salt, ACS Appl. Mater. Interfaces. 7 (2015) 21198–21207. doi:10.1021/acsami.5b05179.

Table captions

Table 1. (**a**) Equivalent circuit used for NNLS analysis of the EIS data (see Fig. 2) and (**b**) related electrode/electrolyte interface resistances (R_i).

Figure captions

Figure 1. Galvanostatic cycling in three-electrodes lithium cells including lithium reference probe of (**a**, **b**) $LiFe_{0.25}Mn_{0.5}Co_{0.25}PO_4$, (**c**, **d**) Sn-C, and (**e**, **f**) Sn-Fe_2O_3-C in terms of (**left** panels) voltage profiles of the 1st, 10th, and 40th cycles and (**right** panels) cycling behavior. For cell preparation see experimental section

Figure 2. (**a-c**) Nyquist plots of EIS tests in three-electrodes lithium cells including lithium reference probe of (**a**) $LiFe_{0.25}Mn_{0.5}Co_{0.25}PO_4$, (**b**) Sn-C, (**c**) Sn-Fe_2O_3-C working electrodes; measurements performed at OCV and after the 1st, 10th, and 40th cycles of galvanostatic cycling (see Fig. 1). For cell preparation see experimental section

Figure 3. Voltage profile of $LiFe_{0.25}Mn_{0.5}Co_{0.25}PO_4$ cathode compared to partially lithiated Sn-C (**a**) and to partially lithiated Sn-Fe_2O_3-C (**b**). Surface geometric capacity of the cells reported in the bottom x-axes, and the corresponding gravimetric capacity of the $LiFe_{0.25}Mn_{0.5}Co_{0.25}PO_4$ cathode in the top x-axes. Current rates: C/10 for $LiFe_{0.25}Mn_{0.5}Co_{0.25}PO_4$ (1C = 170 mA g^{-1}), C/4 for Sn-C (1C = 400 mA g^{-1}), and 1C for Sn-Fe_2O_3-C (1C = 810 mA g^{-1}). (**c**) Voltage profile of the 20th, steady-state cycle for the Sn-C/$LiFe_{0.25}Mn_{0.5}Co_{0.25}PO_4$ and Sn-Fe_2O_3-C/$LiFe_{0.25}Mn_{0.5}Co_{0.25}PO_4$ cells, cycled at C/5 with respect to the cathode mass (1C = 170 mA g^{-1}).

Figure 4. Galvanostatic performances of the Sn-C/$LiFe_{0.25}Mn_{0.5}Co_{0.25}PO_4$ and Sn-Fe_2O_3-C/$LiFe_{0.25}Mn_{0.5}Co_{0.25}PO_4$ cells at C/5 rate with respect to the cathode (1C = 170 mA g^{-1}). Voltage

profiles of the 2nd, 10th, 20th, 30th, and 40th cycles for (**a**) Sn-C/$LiFe_{0.25}Mn_{0.5}Co_{0.25}PO_4$ and (**b**) Sn-Fe_2O_3-C/$LiFe_{0.25}Mn_{0.5}Co_{0.25}PO_4$ cells and (**c**) comparison of the corresponding cycling trends.

Table 1

(a)

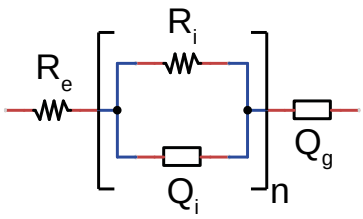

(b)

	$LiFe_{0.25}Mn_{0.5}Co_{0.25}PO_4$				Sn-C				Fe_2O_3-Sn-C			
	R_1 (Ω)	R_2 (Ω)	R_3 (Ω)	R_{tot} (Ω)	R_1 (Ω)	R_2 (Ω)	R_3 (Ω)	R_{tot} (Ω)	R_1 (Ω)	R_2 (Ω)	R_3 (Ω)	R_{tot} (Ω)
OCV	30.1 ± 0.5			30.1 ± 0.5	25.6 ± 0.5			25.6 ± 0.5	52.2 ± 1.0			52.2 ± 1.0
1st cycle	40 ± 30	140 ± 30		180 ± 60	1.9 ± 0.5	6.7 ± 0.9	9.0 ± 0.8	18 ± 2	3 ± 1	4 ± 4	16 ± 6	20 ± 10
10th cycle	238 ± 3			238 ± 3	2.0 ± 0.9	21 ± 3	17 ± 3	40 ± 6	1.9 ± 0.7	4 ± 2	7 ± 2	12 ± 4
40th cycle	425 ± 5			425 ± 5	2.8 ± 1	40 ± 5	42 ± 7	80 ± 10	2 ± 1	7 ± 5	8 ± 5	20 ± 10

Table 1

Figure 1

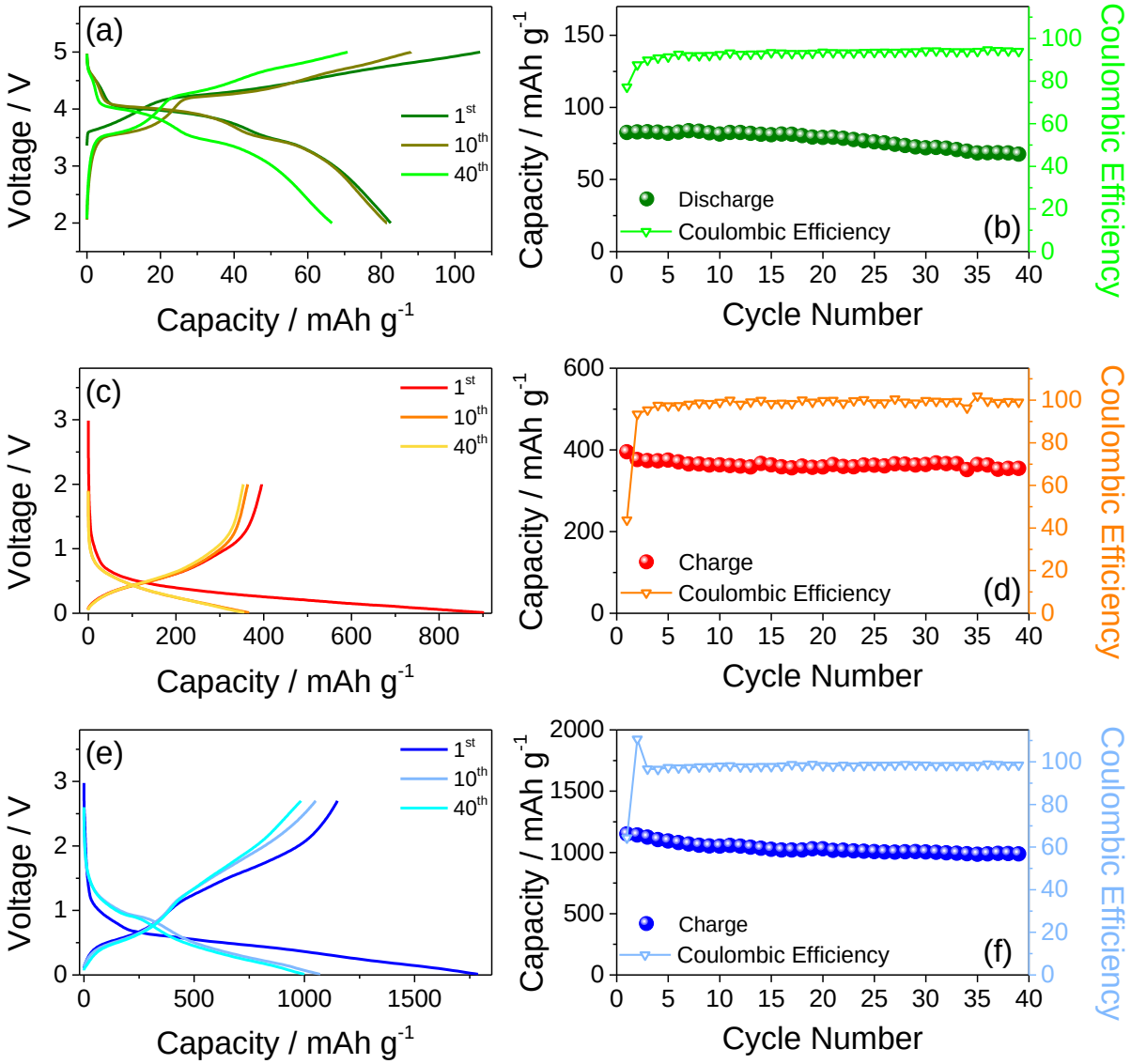

Figure 1

Figure 2

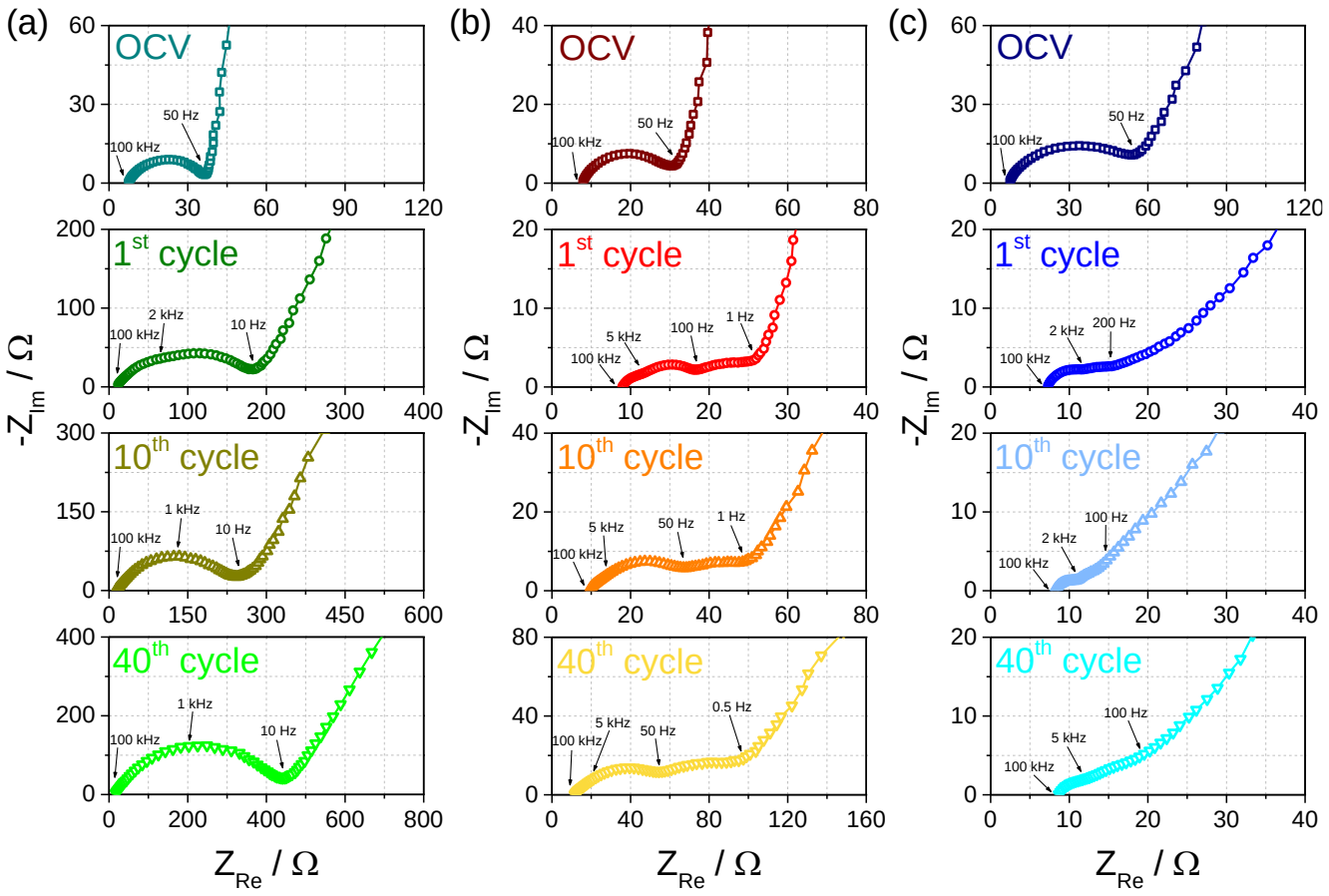

Figure 2

Figure 3

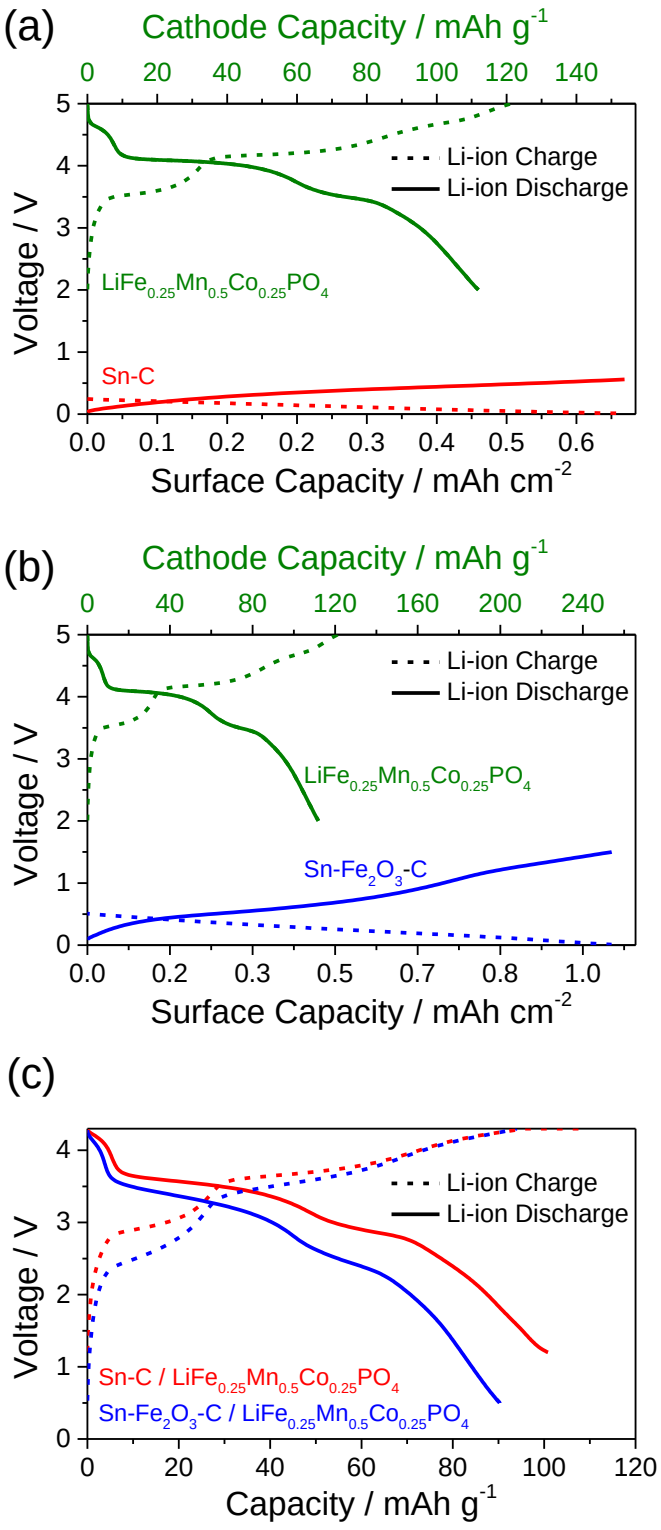

Figure 3

Figure 4

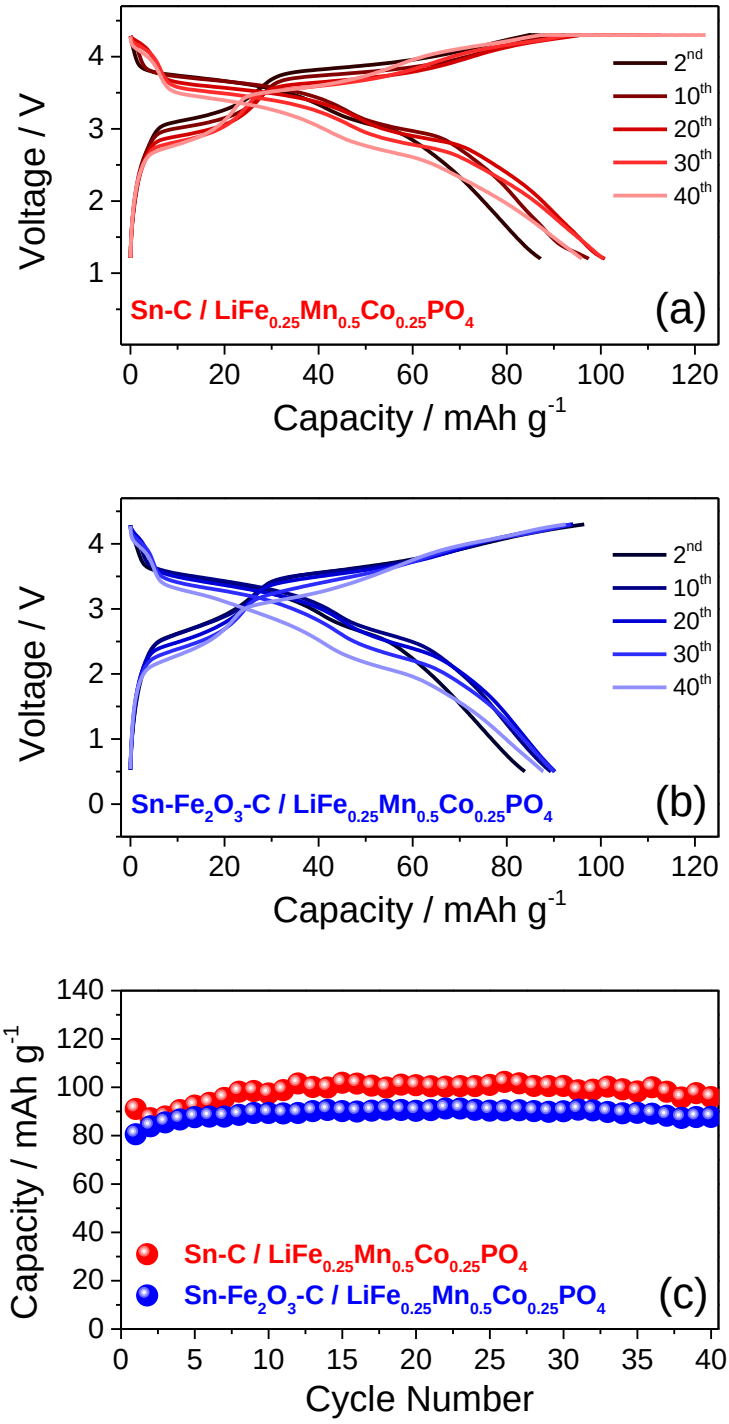

Figure 4